RSC Advances

ROYAL SOCIETY OF CHEMISTRY

www.rsc.org/advances

RSC Advances

ARTICLE

Ultrathin γ-Al_2O_3 nanofibers with large specific surface area and their enhanced thermal stability by Si-doping

Received 00th January 20xx,
Accepted 00th January 20xx

DOI: 10.1039/x0xx00000x

www.rsc.org/

Fang Hu,[a] Xiang Wu,[ac] Yamin Wang[a] and Xiaoyong Lai*[b]

A series of ultrathin boehmite nanofibers with large specific surface area (302~385 $m^2 \cdot g^{-1}$) were synthesized via a parallel flow co-precipitation method by using cheap $NaAlO_2$ and $Al_2(SO_4)_3$ as reactive agents and then transformed into γ-Al_2O_3 by calcination at 500 °C. The resultant γ-Al_2O_3 possess similar nanofibrous morphology with a length of over 100 nm and a transverse size of ~2nm, large specific surface area of up to 419 $m^2 \cdot g^{-1}$ and relatively high thermal stability, which still keep a specific surface area of 132, 104 and 70 $m^2 \cdot g^{-1}$ after being calcined at 1000, 1100 and 1200 °C, respectively. Moreover, the thermal stability could be further improved by doping Si for inhibiting the phase transformation and the specific surface area of Si-doped γ-Al_2O_3 nanofibers could be up to 113 $m^2 \cdot g^{-1}$ at 1200°C and improve their thermal stability.

Introduction

Gamma alumina (γ-Al_2O_3) and its related transition forms (such as δ-Al_2O_3, θ-Al_2O_3), as a group of important industrial materials, are widely used in catalysis, adsorption and separation technology and automobile industries because of their desirable textural properties and surface acid–base properties.[1-7] For some specific applications, such as catalytic conversion of automotive emission gas,[8] diesel catalytic oxidation,[9] catalytic decomposition of propellants for space propulsion,[10] the ability of γ-Al_2O_3 to maintain large specific surface area and abundant catalytically active surface sites at 1100~1200 °C or even higher temperature is of vital importance, which will allow for well-dispersion of active precious metal catalytic components and the enhanced catalytic activity. However, γ-Al_2O_3 is metastable phase and likely to sinter and convert irreversibly into the thermodynamically stable α-Al_2O_3 via δ-Al_2O_3 and θ-Al_2O_3 intermediate phases at elevated temperature.[11-13] These transformations are accompanied by a catastrophic decrease of specific surface area and a change in surface chemistry, which severely affects their usefulness in practical applications.[14] Therefore, it has been attracting great interest to develop a variety of γ-Al_2O_3 with large specific surface area

Since the discovery of MCM-type mesoporous silica, many efforts have been devoted to synthesize mesoporous γ-Al_2O_3 materials as their large specific surface areas could provide much more active sites and regular porosity would be favorable for the diffusion and transport of reactive molecules.[15-23] For examples, Yuan et al. have successfully synthesized an ordered mesoporous γ-Al_2O_3 with large specific surface area of 400 $m^2 \cdot g^{-1}$ via the modified organic-template method, which could maintain its ordered mesostructure with a specific surface area of 116 $m^2 \cdot g^{-1}$ at 1000 °C and suffer from structural collapse above 1100 °C.[24] Jiang et al. have also reported the synthesis of mesoporous La-doped γ-Al_2O_3 with enhanced thermal stability, which maintain a specific surface area of 101 $m^2 \cdot g^{-1}$ at 1200 °C.[25] Besides mesoporous γ-Al_2O_3, nanofibrous γ-Al_2O_3 which could be usually produced from the thermal transformation of boehmite nanofibers, also attracts considerable attention, whose distinctive one-dimensional geometry characteristics and randomly stacking way allow for large specific surface area and large pore volume.[26-28] Zhu et al. reported the synthesis of boehmite nanofibers with a specific surface area of 376 $m^2 \cdot g^{-1}$ under the assistant of nonionic polyethylene oxide (PEO) surfactant[29-30] and the derived γ-Al_2O_3 nanofiber still remains a specific surface area of 68 $m^2 \cdot g^{-1}$, even after being heated at 1200 °C. Peng et al. have synthesized well-crystallized boehmite nanofibers with a specific surface area of 218 $m^2 \cdot g^{-1}$ without use of any surfactant and the derived γ-Al_2O_3 nanofiber after calcined at 500 °C exhibits a specific surface area of 209 $m^2 \cdot g^{-1}$, but decreased to 41 $m^2 \cdot g^{-1}$ after being calcined at 1200 °C.[31] Alphonse et al. have also obtained La-doped nanofibrous γ-Al_2O_3 from boehmite hydrosols containing a triblock copolymer (P123) and lanthanum nitrate, which could keep a specific surface area of about 71 $m^2 \cdot g^{-1}$ at 1200°C.[32] However, there still is a great demand for developing γ-Al_2O_3 with bot

[a] School of Materials Science and Engineering, Shenyang University of Technology, Shenyang 110870, People's Republic of China.
[b] Key Laboratory of Energy Resource and Chemical Engineering, State Key Laboratory Cultivation Base of Natural Gas Conversion, School of Chemistry and Chemical Engineering, Ningxia University, Yinchuan 750021, People's Republic of China. Email: xylai@nxu.edu.cn; Fax: +86 951 2062323; Tel: +86 951 2062861
[c] College of Chemistry and Chemical Engineering, Harbin Normal University, Harbin 150025, People's Republic of China.

† Footnotes relating to the title and/or authors should appear here.
Electronic Supplementary Information (ESI) available: Nitrogen physisorption analysis, additional TEM images, thermal stability data. See DOI: 10.1039/x0xx00000x

larger specific surface area and higher thermal stability via a simple and low-cost method.

Herein, we have successfully synthesized a series of ultrathin boehmite nanofibers with large specific surface area (302~385 $m^2 \cdot g^{-1}$) via a parallel flow co-precipitation method by using cheap $NaAlO_2$ and $Al_2(SO_4)_3$ as reactive agents and then transformed them into γ-Al_2O_3 by calcination at 500 °C. The resultant γ-Al_2O_3 possess similar nanofibrous morphology, large specific surface area of up to 419 $m^2 \cdot g^{-1}$ and relatively high thermal stability, which still keep a specific surface area of 132, 104 and 70 $m^2 \cdot g^{-1}$ after being calcined at 1000, 1100 and 1200 °C, respectively. Moreover, the thermal stability could be further improved by doping Si and the specific surface area of Si-doped γ-Al_2O_3 could be up to 113 $m^2 \cdot g^{-1}$ after being calcined at 1200°C, which is significantly superior over those previously reported in the literatures.

Experimental section

Synthesis of boehmite precursors:

First, $NaAlO_2$ solution (80 $g \cdot L^{-1}$, α_k=1.42) was prepared by adding $Al(OH)_3$ into 300 mL NaOH solution (62 $g \cdot L^{-1}$) at 100 °C. And then, the resultant $NaAlO_2$ solution and $Al_2(SO_4)_3$ solution (342 $g \cdot L^{-1}$) were together dropped into distilled water at 60°C slowly under vigorous magnetic stirring. The white precipitation formed at the required pH value (6~11) and aged for 2h at 90 °C under strong stirring. The solid product was collected by filter and washed by hot water (90 °C) for several times, following dried at 110°C, which are marked as B-*x* (*x*= the corresponding pH value). For comparison, two products were synthesized at the pH value of 9 and washed by using cool water (20 °C) instead of hot water or additionally using ethanol besides hot water before dried.

Synthesis of γ-Al_2O_3:

The as-synthesized boehmite precursors were heated to 500 °C with a constant heating rate of 2 °C·min^{-1} and kept at 500 °C for 4h to decompose boehmite into γ-Al_2O_3, which was marked as A-500.

Synthesis of Si-doped γ-Al_2O_3:

In order to synthesize Si-doped γ-Al_2O_3, a given amount of tetraethyl orthosilicate (TEOS) was added into the as-obtained γ-Al_2O_3 and followed drying for 24h and calcination at 500°C. Five Si-doped γ-Al_2O_3 products with different Si-dopant contents (2 wt%, 4wt%, 6 wt%, 8 wt% and 10 wt%, where the weight content of the Si-dopant was calculated in the form of SiO_2) are synthesized, which were marked as SA-2%, SA-4%, SA-6%, SA-8%, SA-10%, respectively.

Thermal stability investigation:

The above-mentioned γ-Al_2O_3 was heated in air from 500 to 1000, 1100 or 1200 °C at the ramping rate of 10 °C·min^{-1} and kept the temperature for 3h and the resultant products were marked as A-1000, A-1100, A-1200, respectively.

Characterization

X-ray diffraction (XRD) was carried out for phase analysis and crystal structure of calcined powder using XRD-7000 with Cu Kα radiation. A continuous mode was used to collect 2θ date from 10° to 70° with a sampling pitch of 0.02 °·s^{-1}. FTIR spectrum was collected on a Bruker IF S66V FTIR spectrometer in a frequency range of 4000-400cm^{-1} at the frequency step size of 4 cm^{-1}. Transmission electron microscopy (TEM) experiments were conducted on a JEOL-3010 TEM microscope operated at an accelerating voltage of 300kV to investigate the morphology of the material. The nitrogen adsorption-desorption isotherms at the temperature of liquid nitrogen (77 K) were measured on V-Sorb 4800P Surface Area and Pore Porosimetry Analyzer (Gold Spectrum Technology Co., Ltd., China) with prior degassing under vacuum for 4 h at 200 °C. Total pore volumes were determined using the adsorbed volume at a relative pressure of 0.99. The multi-point Brunauer-Emmet-Teller (BET) surface area was estimated from the relative pressure range from 0.05 to 0.2. The pore size distribution of all the materials was analyzed from the desortpiton isotherm using the Barrett-Joyner-Halenda (BJH) method. Energy dispersive X-ray (EDX) pattern was recorded on a scanning electron microscopy (SEM) (Model S-3400N, Hitachi, Japan) attached with an EDX analyzer

Results and discussion

A series of boehmite precursors are firstly synthesized by a parallel flow co-precipitation method and the effect of the pH values was investigated. Fig. 1 presents the XRD patterns of the products prepared at different pH values from 6 to 11. The diffraction peaks of all the products could be readily indexed to a pure boehmite phase (γ-AlOOH, JCPDS, No. 21-1307). With increasing pH values, the reflection peaks become sharp gradually, which indicates the growth of crystalline boehmite γ-AlOOH. The nitrogen adsorption-desorption isotherms and pore size distribution curves of all the boehmite precursors are shown in Fig. 2. Each the precursor exhibits a type IV isotherms with H2 hysteresis loop, representing the existence of slit-like mesopores. With increasing the pH value from 6 to 9, the specific surface area of γ-AlOOH increased from 329 to 361 $m^2 \cdot g^{-1}$ and the total pore volume also increased from 0.60 to

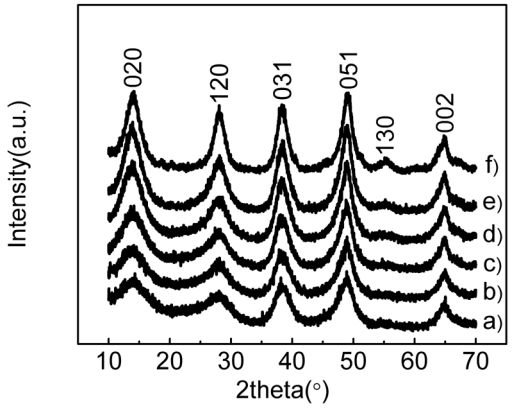

Fig. 1 XRD patterns of boehmite precursors obtained in the different reaction pH values: (a) 6, (b) 7, (c) 8, (d) 9, (e) 10 and (f) 11.

Table 1 Textural properties of boehmite precursors obtained in the different reaction pH values

Product	pH value	S_{BET}($m^2 \cdot g^{-1}$)[a]	V_t($cm^3 \cdot g^{-1}$)[b]	D_p(nm)[c]
B-6	6	329	0.60	4.4
B-7	7	338	0.61	4.2
B-8	8	347	0.64	4.5
B-9	9	361	0.66	4.8
B-10	10	337	0.59	4.8
B-11	11	325	0.41	3.8

[a]Multi-point Brunauer-Emmet-Teller (BET) specific surface area was estimated from the relative pressure range of 0.05 ~ 0.2. [b]Total pore volume was determined using the adsorbed volume at a relative pressure of 0.99.[c]The pore size distribution was calculated from the adsorption branches of the N_2 physisorption isotherms using the Barrett-Joyner-Halenda (BJH) algorithm

0.64 $cm^3 \cdot g^{-1}$. Further increasing the pH value to 10 or 11, both the specific surface area and the total pore volume of the resultant boehmite precursors gradually decreased (see Table 1). Therefore, the optimum pH value for getting large specific surface area boehmite precursors should be 9. Moreover, the washing way have also affected on the textural properties of the resultant boehmite precursors (Fig. S1). When the cool water (20 °C) was used to washing boehmite precursors instead of hot water, the resultant boehmite precursor would exhibit a lower specific surface area and total pore volume (302 m $m^2 \cdot g^{-1}$ and 0.47 $cm^3 \cdot g^{-1}$, respectively). If ethanol besides hot water (90 °C) was additionally used, a product with higher specific surface area and total pore volume (385 $m^2 \cdot g^{-1}$ and 1.18 $cm^3 \cdot g^{-1}$, respectively) could be obtained and the pore size also increased from 9.6 to 20.6 nm. Typical TEM images for the boehmite product obtained at the pH value of 9 and washed by hot water (90 °C) and ethanol are shown in Fig. 3. The lower magnified image (Fig. 3a) clearly exhibits that the as-synthesized boehmite product consist of some continuous nanofibers with a length of over 100 nm and there exist some large textural mesopores among these disordered stacking nanofibers, in agreement with its pore size distribution data. The higher magnified image (Fig. 3b) reveals that these nanofibers possess a very thin transverse size of ~2 nm, which

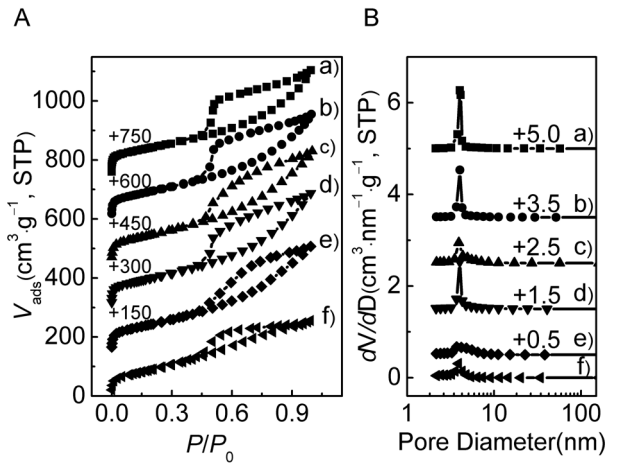

Fig. 2 (A) Nitrogen adsorption-desorption isotherms and (B) the corresponding pore size distribution curves of boehmite precursors obtained in the different reaction pH value: (a) 6, (b) 7, (c) 8, (d) 9, (e) 10 and (f) 11.

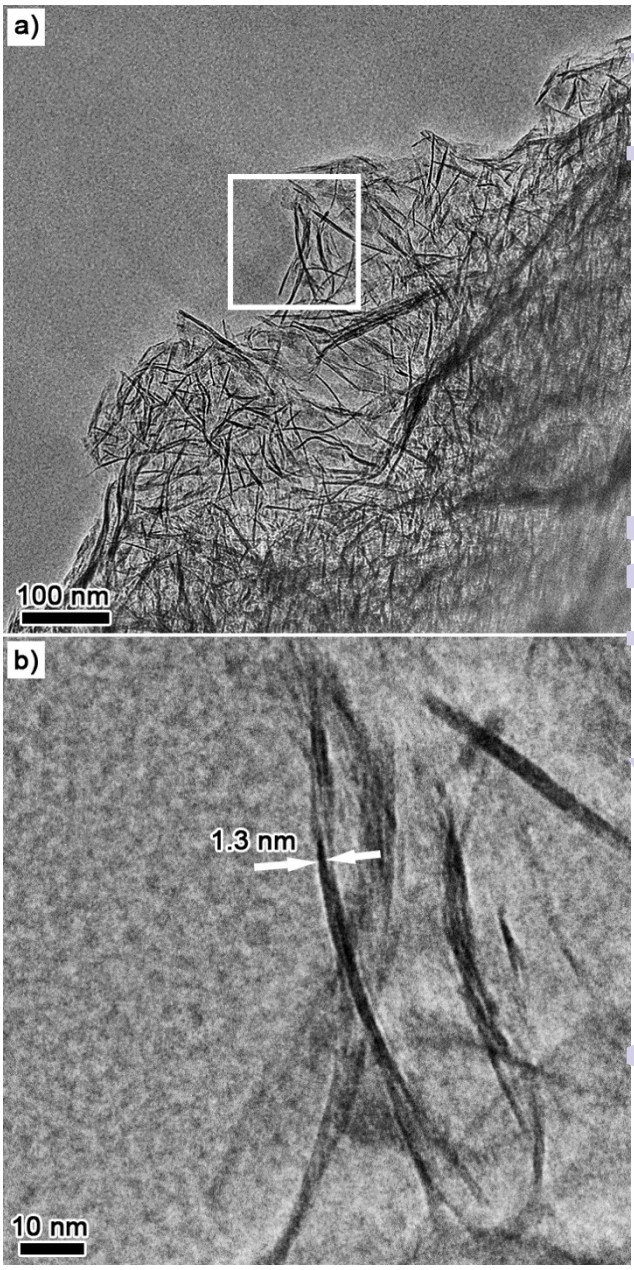

Fig. 3 TEM images of the boehmite product obtained at the pH value of 9 and washed by hot water (90 °C) and ethanol: (a) lower magnification, (b) higher magnification of the area indicated by white frame in (a).

thus endow them large specific surface area.

By calcination at 500 °C, the above-mentioned boehmite nanofibers could be easily transformed into the corresponding alumina, whose XRD pattern is shown in Fig. 4a. Three reflection peaks at 2θ=37.1, 46.0 and 66.6° could be clearly observed, which could correspond to the reflections of the (311), (400) and (440) planes of γ-Al_2O_3 (JCPDS, No. 10-0425), respectively. TEM image (Fig. 5a and Fig. S2) reveals the obtained γ-Al_2O_3 product consist of some disordered stacking nanofibers with a length of over 100 nm and a transverse size of ~2 nm, which is very similar with their boehmite precursors (Fig. 3). Porosity measurement was performed using nitrogen physisorption at 77 K and the γ-Al_2O_3 nanofibers exhibits a

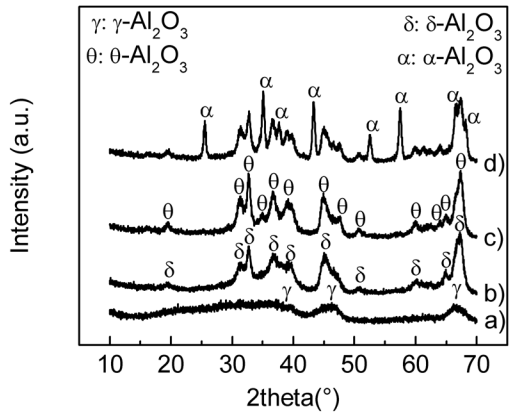

Fig. 4 XRD patterns of alumina obtained at different calcined temperatures: (a) 500 °C, (b) 1000 °C, (c) 1100 °C and (d) 1200 °C

large specific surface area of 419 $m^2 \cdot g^{-1}$ and total pore volume of 1.6 $cm^3 \cdot g^{-1}$ as well as narrow pore size distribution centered at 9.5 nm (Fig. 6 and Table 2). The investigation on the thermal stability of the γ-Al_2O_3 nanofibers was also carried out by calcination at high temperature (1000~1200 °C) and a sequent phase transformation from γ-Al_2O_3 to δ-Al_2O_3, θ-Al_2O_3 and α-Al_2O_3 could be observed at their XRD patterns with increasing calcination temperature (Fig. 4). Companied with phase transformation, the nanofiber gradually became shorter in length and larger in transverse size (Fig. 5b-d). As a result, the specific surface area decreased to 132, 104 and 70 $m^2 \cdot g^{-1}$ at 1000, 1100 and 1200 °C respectively (Fig. 6 and Table 2) and the total pore volume also decreased to 0.91, 0.55 and 0.51 $cm^3 \cdot g^{-1}$ respectively. These results confirmed our products possess a better thermal stability than those fibrous alumina reported in the literatures[30-31] and are also comparable with its

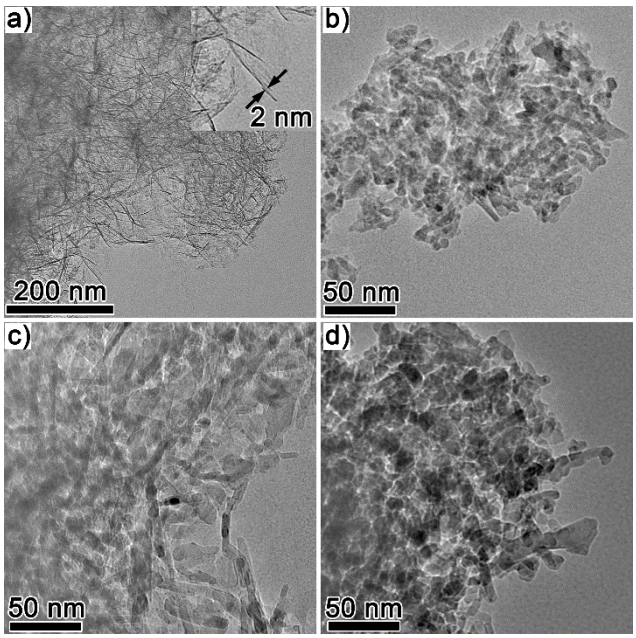

Fig. 5 TEM images of alumina obtained at different calcined temperatures: (a) 500 °C, (b) 1000 °C, (c) 1100 °C and (d) 1200 °C.

Table 2 Textural properties of γ-Al_2O_3 nanofibers and Si-doped γ-Al_2O_3 nanofibers after calcined at different temperatures.

Product	Calcined temperature (°C)	$S_{BET}(m^2 \cdot g^{-1})^a$	$V_t(cm^3 \cdot g^{-1})^b$	$D_P(nm)^c$
A-500	500	419	1.60	9.6
A-1000	1000	132	0.91	17.9
A-1100	1100	104	0.55	19.5
A-1200	1200	70	0.51	20.6
SA-2%	1200	87	0.43	14.9
SA-4%	1200	101	0.56	17.5
SA-6%	1200	113	0.69	17.0
SA-8%	1200	102	0.59	14.6
SA-10%	1200	92	0.56	16.6

[a]Multi-point Brunauer-Emmet-Teller (BET) specific surface area was estimated from the relative pressure range of 0.05 ~ 0.2. [b]Total pore volume was determined using the adsorbed volume at a relative pressure of 0.99.[c]The pore size distribution was calculated from the adsorption branches of the N_2 physisorption isotherms using the Barrett-Joyner-Halenda (BJH) algorithm

La-doped counterpart[32], see Table S1.

In addition, the Si dopant was introduced into the γ-Al_2O_3 nanofibers in order to further enhance their thermal stability by using TEOS as Si sources and the effect of the Si dopant content was investigated. The XRD patterns of all the Si-doped γ-Al_2O_3 nanofibers after calcination at 1200°C for 3h in air were shown in Fig. 7. Compared with the reflection peaks corresponding to θ-Al_2O_3, those corresponding to α-Al_2O_3 gradually became weaker with increasing the Si dopant content, suggesting a reduction of α-Al_2O_3 content in the resultant products. When the Si dopant content is over 6 wt%, no any reflection peaks corresponding to α-Al_2O_3 could be observed from the corresponding XRD patterns, suggesting the absence of the considerable amount of α-Al_2O_3. Similar result are also observed at their FTIR spectra shown in Fig. 8. Two important bands at 567 and 830 cm^{-1} resulting from the stretching modes of octahedral alumina (AlO_6) and tetrahedral aluminum (AlO_4) could be obvious at all the FTIR spectra, whereas another two bands at 444 and 582 cm^{-1} assigned to

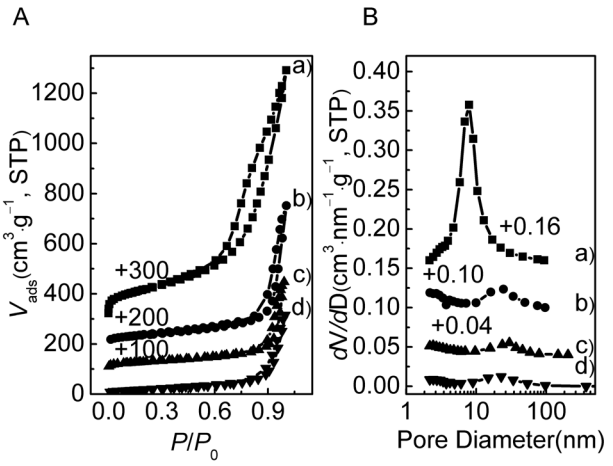

Fig. 6 (A) Nitrogen adsorption-desorption isotherms and (B) the corresponding pore size distribution curves of alumina obtained at different calcined temperatures: (a) 500 °C, (b) 1000 °C, (c) 1100 °C and (d) 1200 °C

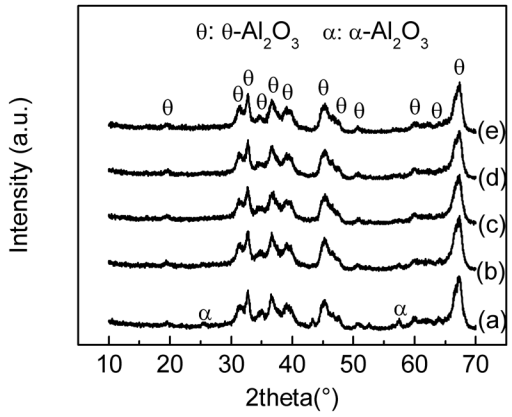

Fig. 7 XRD patterns of the Si-doped γ-Al2O3 nanofibers with different Si-dopant contents after being calcined at 1200°C: (a) 2 wt%, (b) 4 wt%, (c) 6 wt%, (d) 8 wt% and (e) 10 wt%.

the stretching of Al-O bands of α-Al_2O_3 could be only observed at the FTIR spectra of the Si-doped γ-Al_2O_3 nanofibers with Si-dopant content of 2 wt% and 4 wt%. Combined with XRD and FTIR data, we could conclude that the introduction of Si dopant effectively inhibits the phase transformation to α-Al_2O_3. As a result, the thermal stability of the Si-doped γ-Al_2O_3 nanofibers are significantly improved, which could maintain larger specific surface area at 1200°C (Fig. 9 and Table 2), compared with the pure γ-Al_2O_3 nanofibers. When the Si dopant content is 6 wt%, the Si-doped γ-Al_2O_3 nanofibers exhibit a highest specific surface area of 113 $m^2 \cdot g^{-1}$, which is larger than that of mesoporous La-doped γ-Al_2O_3 [25], see Table S1. The EDX result shows that the weight content of Si-dopant in the resultant material is about 5.6 wt%, which is consistent with the given value (Fig. S3). Further increasing the Si dopant content, the specific surface area of the resultant products gradually decrease, possibly due to the pore block derive from excess Si dopant products or the generation of large Si dopant products.

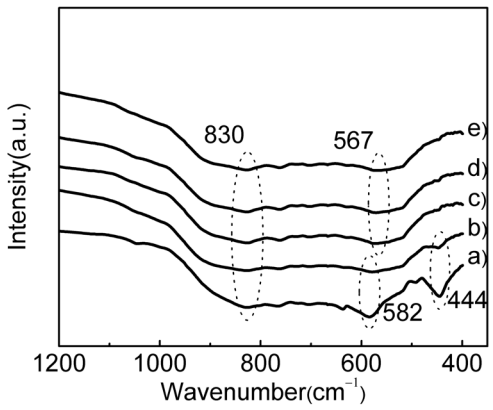

Fig. 8 FTIR spectra of the Si-doped γ-Al_2O_3 nanofibers with different Si-dopant contents after being calcined at 1200°C: (a) 2 wt%, (b) 4 wt%, (c) 6 wt%, (d) 8 wt% and (e) 10 wt%.

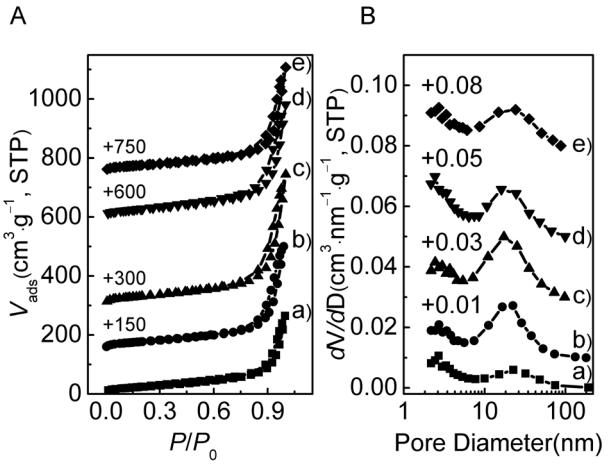

Fig. 9 (A) Nitrogen adsorption-desorption isotherms and (B) the corresponding pore size distribution curves of the Si-doped γ-Al_2O_3 nanofibers with different Si-dopant contents after being calcined at 1200°C: (a) 2 wt%, (b) 4 wt%, (c) 6 wt%, (d) 8 wt% and (e) 10 wt%.

Conclusions

In summary, we have successfully synthesized a series of boehmite with large specific surface area via a simple parallel flow co-precipitation method by using cheap $NaAlO_2$ and $Al_2(SO_4)_3$ as reactive agents and then transformed them into γ-Al_2O_3 by calcination. The resultant γ-Al_2O_3 possess unique nanofibrous morphology, large specific surface area of up to 419 $m^2 \cdot g^{-1}$ and relatively high thermal stability. The thermal stability was further enhanced by introducing Si-dopant and the as-obtained Si-doped γ-Al_2O_3 nanofibers could maintain a large specific surface area of up to 113 $m^2 \cdot g^{-1}$ at 1200 °C. Such a unique nanofibrous material with both large specific surface area and high thermal stability will find application as a high-temperature catalyst or catalyst support in the automotive and petroleum industries.

Acknowledgements

This work was partly supported by the National Natural Science Foundation of China (No. 51362024, and 21006116), the Natural Science Foundation of Ningxia of China (No. NZ12111), the Chinese Ministry of Science & Technology. Xiaoyong Lai thanks the West Light Foundation of The Chinese Academy of Sciences.

Notes and references

1 A. Martinez, G. Prieto and J. Rollan, *J. Catal.*, 2009, **263**, 292.
2 X. Wang, Y. Guo, G. Lu, Y. Hu, L. Jiang. Y. Guo and Z. Zhang, *Catal. Today*, 2007, **126**, 369.
3 Y. Wang, W. Li, X. Jiao and D. Chen, *J. Mater. Chem. A*, 2013, **1**, 10720.
4 Y. Sang, Q. Gu, T. Sun, F. Li and C. Liang, *J. Hazard. Mater.*, 2008, **153**, 860.
5 Z. G. Zhao, N. Nagai, T. Kodaira, Y. Hukuta, K. Bando, I. Takashima and F. Mizukami, *J. Mater. Chem.*, 2011, **21**, 14984.

6 K. Keyvanloo, M. K. Mardkhe, T. M. Alam, C. H. Bartholomew, B. F. Woodfield and W. C. Hecker, *ACS Catal.*, 2014, **4**, 1071.
7 S. C. Shen, W. K. Ng, Q. Chen, X. T. Zeng, M. Z. Chew and R. B. H. Tan, *J. Nanosci. Nanotechnol.*, 2007, **7**, 2726.
8 M. Shen, M. Yang, J. Wang, J. Wen, M. Zhao and W. Wang, *J. Phys. Chem. C*, 2009, **113**, 3212.
9 F. Zhong, Y. Zhong, Y. Xiao, G. Cai and K. Wei, *Catal. Lett.*, 2011, **141**, 1828.
10 S. Zhu, X. Wang, A. Wang and T. Zhang, *Catal. Today*, 2008, **131**, 339.
11 C. Legros, C. Carry, P. Bowen and H. Hofmann, *J. Eur. Ceram. Soc.*, 1999, **19**, 1967.
12 P. Burtin, J. P. Brunelle, M. Pijolat and M. Soustelle, *Appl. Cataly.*, 1987, **34**, 225.
13 H.J. Youn, J. W. Jang, I. T. Kim and K. S. Hong, *J. Colloid Interface Sci.*, 1999, **211**, 110.
14 B. Djuricic, S. Pickering, P. Glaude, D. McGarry and P. Tambuyser, *J. Mater. Sci.*, 1997, **32**, 589.
15 X. Y. Lai, X. T. Li, W. C. Geng, J.C. Tu, J. X. Li and S. L. Qiu, *Angew. Chem. Int. Ed.*, 2007, **46**, 738-741.
16 Q. Wu, F. Zhang, J. Yang, Q. Li, B. Tu and D. Zhao, *Microporous Mesoporous Mater.*, 2011, **143**, 406.
17 W. Li and D. Y. Zhao, *Chem. Commun.*, 2013, **49**, 943.
18 S. A. Bagshaw, E. Prouzet and T. J. Pinnavaia, *Science*, 1995, **269**, 1242.
19 S. A. Bagshaw and T. J. Pinnavaia, Angew. *Chem.-Int. Edit. Engl.*, 1996, **35**, 1102.
20 P. D. Yang, D.Y. Zhao, D. I. Margolese, B. F. Chmelka and G. D. Stucky, *Chem. Mater.*, 1999, **11**, 2813.
21 Z. Y. Yuan, T. Z. Ren, A. Azioune, J. J. Pireaux and B. L. Su, *Chem. Mater.*, 2006, **18**, 1753.
22 P. Bai, P. P. Wu, Z.F. Yan and X. S. Zhao, *Microporous Mesoporous Mater.*, 2009, **118**, 288.
23 J. P. Dacquin, J. Dhainaut, D. Duprez, S. Royer, A. F. Lee and K. Wilson, *J. Am. Chem. Soc.*, 2009, **131**, 12896.
24 Q. Yuan, A. X. Yin, C. Luo, L. D. Sun, Y. W. Zhang, W. T. Duan, H. C. Liu and C. H. Yan, *J. Am. Chem. Soc.*, 2008, **130**, 3465.
25 L. Jiang, Y. Wang, X. Wang, Y. Luo, Y. Cao and K. Wei, *J. Rare Earth.*, 2013, **31**, 1081.
26 S. C. Kuiry, E. Megen, S. D. Patil, S. A. Deshpande and S. Seal, *J Phys. Chem. B*, 2005, **109**, 3868.
27 S. C. Shen, W. K. Ng, Z. Y. Zhong, Y. C. Dong, L. Chia and R. B. Tan, *J. Am. Ceram. Soc.*, 2009, **92**, 1311.
28 X. Ke, Y. Huang, T. R. Dargaville, Y. Fan, Z. Cui and H. Zhu, *Sep. Purif. Technol.*, 2013, **120**, 239.
29 H. Zhu, X. Gao, D. Song, Y. Bai, S. Ringer, Z. Gao, Y. Xi, W. Martens, J. Riches and R.L. Frost, *J. Phys. Chem. B*, 2004, **108**, 4245.
30 H. Y. Zhu, J. D. Riches and J. C. Barry, *Chem. Mater.*, 2002, **14**, 2086.
31 L. Peng, X. Xu, Z. Lv, J. Song, M. He, Q. Wang, L. Yan, Y. Li and Z. Li, *J. Therm. Anal. Calorim.*, 2012, **110**, 749.
32 P. Alphonse and B. Faure, *Microporous Mesoporous Mater.*, 2014, **196**, 191.